Identification of a Small-Molecule Modulator of Astrocyte Reactivity for Optic Nerve Protection

Ting Li,[1–3] Haotian Peng,[1–3] Nanxin Wu,[1–3] Miyao Zhu,[1–3] Ziwei Li,[1–3] Qin Dai,[1–3] Ming Jin,[1–3] Shaohui Pan,[1–3] and Wencan Wu[1–4]

[1]Eye Research Center, Hangzhou Institute of Medicine, Chinese Academy of Sciences, Eye Hospital, Wenzhou Medical University, Hangzhou, People's Republic of China
[2]Zhejiang Key Laboratory of Key Technologies for Visual Pathway Reconstruction, Eye Hospital, Wenzhou Medical University, Wenzhou, Zhejiang, People's Republic of China
[3]State Key Laboratory of Eye Health, Eye Hospital, Wenzhou Medical University, Wenzhou, People's Republic of China
[4]Oujiang Laboratory (Zhejiang Lab for Regenerative Medicine, Vision, and Brain Health), Eye Hospital, Wenzhou Medical University, Wenzhou, People's Republic of China

Correspondence: Wencan Wu, Eye Research Center, Hangzhou Institute of Medicine, Chinese Academy of Sciences, 150 Fuchang Rd., Qiantang District, Hangzhou 310018, People's Republic of China; wuwencan@wmu.edu.cn.
Shaohui Pan, Eye Research Center, Hangzhou Institute of Medicine, Chinese Academy of Sciences, Hangzhou 310018, People's Republic of China; panshaohui2007@126.com.

Received: October 22, 2025
Accepted: April 20, 2026
Published: May 29, 2026

Citation: Li T, Peng H, Wu N, et al. Identification of a small-molecule modulator of astrocyte reactivity for optic nerve protection. *Invest Ophthalmol Vis Sci.* 2026;67(5):73. https://doi.org/10.1167/iovs.67.5.73

Purpose. Injury of the optic nerve leads to retinal ganglion cells (RGCs) apoptosis and irreversible vision loss, in which reactive astrocytes play a central role. The aim of this study is to modulate pathological reactive astrocytes to reduce the progression of optic nerve degeneration.

Methods. Given the therapeutic potential of small molecules to modulate astrocyte reactivity, we used a drug-screening platform to identify small molecules, and evaluated their capacity to regulate astrocyte phenotypes and preserve RGCs after optic nerve crush (ONC). The primary astrocytes from neonatal C57BL/6J mouse cortices, A1 astrocytes, are induced by TNF, IL-1α, and C1q (TIC), both of them are confirmed at transcript and protein levels. High-throughput screening using SiPer, a computational screening platform, together with DRUG-seq2, yielding candidate small molecules, whose effects on A1/A2 transitions were assessed by RT-qPCR, RNA sequencing (RNA-seq), Western blotting, and immunofluorescence. In vivo, an ONC model received intravitreal compound delivery. RGC survival and astrocyte phenotypes were evaluated by retinal flat-mounts and immunofluorescence.

Results. Primary astrocytes exposed to TIC acquired A1 phenotype, characterized by upregulated C3, GBP2, H2-d1, and H2-t23, and induced RGC cytotoxicity. Transcriptomic drug screening identified proteasome inhibition as a potential strategy to suppress pathological reactive astrocytes. Marizomib, a blood-brain barrier (BBB)-permeable proteasome inhibitor, downregulated A1 markers and upregulated A2 neuroprotective genes. In an ONC model, Marizomib reduced GBP2-positive astrocytes and, at a lower dose, a modest increase in RGC survival was observed at 14 days post-ONC.

Conclusions. We developed a small-scale drug-screening platform and identified Marizomib as a modulator of astrocyte phenotypes. Its therapeutic potential was validated both in vitro and in vivo, providing a new chemical tool to modulate astrocyte reactivity for future therapeutic exploration.

Keywords: astrocytes, small-molecule compounds, optic nerve injury, neuroprotection

Traumatic optic neuropathy (TON) is a severe, vision-threatening condition resulting from sudden blunt trauma to the frontal or temporal regions, leading to optic nerve injury. The primary pathological features of TON are retinal ganglion cell (RGC) apoptosis and axonal degeneration.[1] Current treatment options for TON include conservative management, pharmacotherapy (e.g. corticosteroids), or a combined pharmacological and surgical interventions, such as optic canal decompression.[2] However, these approaches have limited efficacy, and most patients experience profound vision loss or complete blindness.[1,3] Therefore, there is an urgent need to develop novel and effective therapeutic strategies for TON. The pathogenesis of TON involves multiple mechanisms, including disruption of the neurovascular unit, microvascular hemorrhage or occlusion, and mechanical compression from optic canal fractures. These events contribute to elevated intra-canalicular pressure and the formation of a hostile microenvironment.[4] Reactive glial cells within this environment release high levels of pro-inflammatory mediators, amplifying secondary inflammatory damage. In particular, persistent activation of astrocytes and microglia promotes glial scar formation and creates an inhibitory environment that impedes axonal survival and regeneration.[5,6] This inflammatory cascade is a major driver of microenvironmental deterioration, ultimately resulting in failed axonal regrowth and impeding the optic

nerve, which is a critical conduit for transmitting visual information from the retina to the brain and consists of the axons of RGCs. Thus, preserving RGC viability is essential for both structural and functional recovery of the optic nerve.[7]

Astrocytes constitute approximately 30% of the total cell population in the mammalian central nervous system (CNS), making them the predominant glial cell type.[8] During brain development, astrocytes play essential roles in neural circuit formation by guiding the establishment, maturation, and pruning of synaptic connections.[9] In the mature CNS, they maintain neuronal microenvironmental homeostasis through neurotransmitter recycling, preservation of blood-brain barrier (BBB) integrity, and regulation of ionic balance.[10] Astrocytes can also sense increased neuronal activity, modulate intracellular Ca^{2+} concentrations, and subsequently release neurotransmitters such as glutamate.[11] Therefore, astrocytes are indispensable for CNS development, synaptic plasticity, and homeostasis. Early transcriptomic studies of reactive astrocytes isolated from ischemic stroke and neuroinflammatory mouse models have identified two distinct phenotypes: the neurotoxic A1 subtype and the neuroprotective A2 subtype.[12] Studies have shown that A1 astrocytes exhibit impaired clearance of synaptic debris and myelin fragments, whereas promoting the death of RGCs and mature oligodendrocyte.[13] Recent studies have highlighted the complexity and heterogeneity of reactive astrocytes in response to CNS injury,[14] and suggests that reactive astrocytes exhibit a spectrum of molecular and functional states that cannot be adequately captured by simple binary classifications. Nevertheless, modulating specific transcriptional and functional programs associated with astrocyte reactivity remains a promising therapeutic strategy. Previous studies have demonstrated that altering astrocyte polarization – such as converting neurotoxic A1 astrocytes into protective A2 astrocytes – through gene overexpression or knockout can protect the CNS. For example, overexpression of Homer1 inhibits A1 astrocyte transformation and attenuates inflammation after intracerebral hemorrhage,[15] whereas the growth factor MFG-E8 regulates A1/A2 polarization.[16] Similarly, Ror2 knockdown reverses the A1/A2 ratio in reactive astrocytes, alleviating mechanical and cold allodynia in rats following thoracotomy.[17]

Small-molecule compounds have been reported to induce cellular reprogramming without altering genetic material.[18,19] Compared with transcription factor (TF)-based approaches, small molecules offer advantages in tunability (dose, timing, and combination), cell permeability, and cost-effectiveness.[20,21] Moreover, small-molecule-based strategies avoid risks associated with genetic manipulation, such as long-term TF expression, inflammation, and insertional mutagenesis.[22]

In this study, we used the SiPer platform in combination with high-throughput drug screening (DRUG-seq2) to identify small molecules capable of modulating astrocyte states.[23,24] Compared with conventional screening methods, artificial intelligence (AI)-based compound prediction harnesses large-scale datasets to efficiently prioritize candidate molecules, while high-throughput screening enables rapid evaluation of compound efficacy in vitro. By integrating these two approaches, we identified a small molecule that suppresses pro-inflammatory astrocyte activation while promoting expression of protective markers. Functional validation in both in vitro and in vivo models confirmed its biological activity. Our findings provide a novel strategy for targeting astrocytes in optic nerve injury and establish a framework for small-molecule drug discovery guided by AI and high-throughput screening. These results may open new avenues for therapeutic interventions and clinical translation in the treatment of optic nerve injury.

Methods

Extraction and Purification of Cortical Astrocytes

Pregnant C57BL/6J mice (Charles River, China) were used to obtain P3 to P5 pups. After meninges removal, cortices were dissected and dissociated with the papain dissociation system (Worthington, 9035-81-1, USA) following the manufacturer's protocol. Single-cell suspensions were seeded on poly-L-ornithine–coated dishes (Sigma-Aldrich, P3655, USA) in DMEM/F12 (Thermo Fisher Scientific, 11320033, USA) supplemented with N2, B27, GlutaMAX, penicillin-streptomycin (all Thermo Fisher Scientific), and 20 ng/mL FGF-2 (R&D Systems) for 24 hours. Cells were then cultured in enrichment medium (1:1 DMEM and neuronal medium) with GlutaMAX, sodium pyruvate, N2, 5 µg/mL N-acetylcysteine (Sigma-Aldrich, A8199, USA), Pen-Strep, 5 ng/mL HB-EGF, 10 ng/mL CNTF, 10 ng/mL BMP4, and 20 ng/mL FGF-2 (all R&D Systems). For experiments, frozen astrocytes were thawed and maintained for 48 hours in medium (1:1 DMEM and Neurobasal) containing GlutaMAX, sodium pyruvate, N2, N-acetylcysteine, 5 ng/mL HB-EGF, 10 ng/mL CNTF, 50 ng/mL BMP4, and 20 ng/mL FGF-2, then switched to Neural Substrate Medium with 5 ng/mL HB-EGF for 72 hours.

Preparation of Whole Retinal Dissociates

Pregnant C57BL/6J mice (Charles River, China) were used to obtain P3 to P5 pups. Eyes were enucleated, and retinas were dissected, minced with a sterile blade, and dissociated into single-cell suspensions using the Papain Dissociation System (Worthington, 9035-81-1, USA) according to the manufacturer's instructions. After centrifugation, the pellet was resuspended in RGC basal medium consisting of Neurobasal medium supplemented with Pen-Strep, NEAA, B27, 20 ng/mL BDNF, and 10 ng/mL NGF for subsequent experiments.

Astrocyte Coculture With Whole Retinal Dissociates

Retinal dissociates were prepared as described above (containing a mixed population of retinal cells, including RGCs) and seeded onto PLO-coated plates precultured with either physical or TNF, IL-1α, and C1q (TIC)-induced astrocytes. Astrocytes were pretreated with cytokine-containing or cytokine-free medium for 24 hours, washed with RGC basal medium, and then overlaid with single cell suspension of whole retinal dissociates. Co-cultures were maintained in RGC basal medium for 24 hours. Then, the cells were fixed in 4% paraformaldehyde (PFA) and immunostaining for RBPMS and TUJ1. Images were acquired using a Zeiss confocal microscope and analyzed with ImageJ software.

Predicting and Screening Small Molecules Using Computation Screening Platform - SiPer

To identify chemical compounds targeting TFs involved in astrocyte reactivity, we applied the SiPer computational

Investigative Ophthalmology & Visual Science

platform.[23] SiPer integrates a manually curated non-cancer perturbation compendium (NCPC) with single-cell RNA sequencing (scRNA-seq) data, enabling the prioritization of signaling proteins and chemical perturbagens. The scRNA-seq data used in this analysis, accessible under GEO accession GSE237675, were published by Cameron et al.,[25] providing the initial and target cellular state required for SiPer analysis. The SiPer platform operates in three key stages:

1) Signaling protein selection: Candidate signaling proteins are first selected from the NCPC by assessing the similarity between user-defined target TFs and the perturbation-induced TF expression changes. This stage involves the identification of signaling proteins whose expression profiles correlate with the target TFs, establishing a foundation for subsequent screening.
2) Prior knowledge network (PKN) integration with scRNA-seq data: In the second stage, SiPer utilizes a PKN to contextualize the identified signaling proteins within the specific astrocyte state captured in the scRNA-seq data. This filtering step ensures that only those signaling proteins relevant to the reactive astrocyte state are retained, facilitating the identification of key molecular targets for regulation.
3) Grouping of signaling proteins and chemical perturbagen identification: The signaling proteins are then grouped according to their respective pathways, as defined by Reactome. Based on target protein similarity, SiPer identifies chemical perturbagens that modulate these signaling proteins. This stage ultimately prioritizes chemical compounds that influence TFs associated with neuroprotective astrocyte phenotypes, offering potential therapeutic strategies for gliotherapy.

By utilizing this integrative approach, SiPer facilitates the identification of small molecules capable of modulating TFs implicated in astrocyte reactivity, thereby supporting the design of targeted therapeutic interventions aimed at modulating astrocyte behavior in neurological diseases.

Quantitative RT-PCR Analysis

Total RNA was extracted from cultured cells using TRIZol reagent (Invitrogen, 15596026CN, USA) following the manufacturer's protocol. RNA concentration was determined with NanoDrop (Thermo Fisher Scientific). Reverse transcription was performed using 1 ug total RNA with HiScript III RT SuperMix for qPCR (+ gDNA Wiper; Vazyme, R323-01, China). RT-qPCR was carried out on a CFX96 Touch Real-Time PCR Detection System (Bio-Rad) using SYBR Master Mix (Vazyme, R323-01, China). The mRNA expression levels were normalized to Gapdh. Primer sequences are listed in Supplementary Table S1.

Immunofluorescence Analysis

Sterile glass coverslips (NEST, 801008, China) were placed in 24-well plates, coated with poly-L-lysine (20 µg/mL) overnight at 4°C, and rinsed 3 times with PBS before cell seeding. Cultured cells were washed with PBS and fixed in 4% PFA for 10 minutes at room temperature, and then permeabilized and blocked with PBS containing 0.3% Triton X-100 and 10% BSA for 1 hour. Cells were incubated overnight at 4°C with primary antibodies diluted in PBS containing 3% BSA. After 3 PBS washes, Alexa Fluor 488- or 594-conjugated secondary antibodies (Invitrogen, USA) were applied for 2 hours at room temperature in the dark, followed by DAPI staining (Beyotime, C1005, China) for 5 minutes. Coverslips were washed, mounted with antifade medium (Beyotime, P0126, China), sealed, and imaged using a Zeiss confocal microscope with ZEN Blue software (version 3.8, Zeiss).

Bulk RNA-Seq Sample Preparation and Analysis

Total RNA was extracted using TRIzol reagent (Invitrogen, USA) following the manufacturer's protocol. RNA concentration and purity were assessed with NanoDrop ND-1000 (NanoDrop, USA), and integrity was confirmed by Bioanalyzer 2100 (Agilent, USA; RIN > 7.0) and denaturing agarose gel electrophoresis. Poly(A) RNA was purified from 1 µg total RNA using Dynabeads Oligo(dT)25-61005 (Thermo Fisher, USA) in 2 rounds, then fragmented at 94°C for 5 to 7 minutes with Magnesium RNA Fragmentation Module (NEB, USA). The cDNA was synthesized with SuperScript II Reverse Transcriptase (Invitrogen, USA), followed by U-labeled second-strand synthesis using *Escherichia coli* (*E. coli*) DNA polymerase I (NEB, USA), RNase H (NEB, USA), and dUTP (Thermo Fisher, USA). After A-tailing, indexed adapters with T-overhangs were ligated, and size selection was performed using AMPure XP beads. Heat-labile UDG (NEB, USA) was applied to remove U bases, and libraries were amplified by PCR (95°C, 3 minutes; 8 cycles of 98°C, 15 seconds; 60°C, 15 seconds; 72°C, 30 seconds; and final extension 72°C, 5 minutes). The average insert size was 300 ± 50 bp. Libraries were sequenced (2 × 150 base pair [bp], PE150) on an Illumina NovaSeq 6000 (LC-Bio Technology, China). Raw reads were processed with fastp (https://github.com/OpenGene/fastp) to remove adapters, low-quality bases, and undetermined reads. Clean reads were aligned to the human genome (GRCh38) using HISAT2 (https://ccb.jhu.edu/software/hisat2). Transcripts were assembled with StringTie (https://ccb.jhu.edu/software/stringtie) and merged with gffcompare (https://github.com/gpertea/gffcompare) to generate a comprehensive transcriptome. Expression levels were estimated as FPKM (FPKM = [total_exon_fragments/mapped_reads (millions) × exon_length(kb)]) using StringTie. Differentially expressed mRNAs were identified with edgeR (https://bioconductor.org/packages/release/bioc/html/edgeR.html) based on fold change > 2 or < 0.5 and parametric F-test ($P < 0.05$).

Cell Sample Preparation and DRUG-Seq2

The source of primary cell and culture methods are as described above, before collection for DRUG-seq, after 1 hour of pretreatment with different small-molecule compounds, cells were co-incubated with TIC medium or basal medium for 24 hours, after which samples were collected according to DRUG-seq sampling standards. All small-molecule compounds used in the experiment were purchased from TargetMol (China).

Drug-seq2 was performed by Plastech Pharmaceutical Technology Co., Ltd. using the Elite CellSignature High-Throughput 3′ Transcriptome Kit (Plastech), as previously described. Data were processed following the Drop-seq protocol (https://github.com/broadinstitute/Drop-seq).

Investigative Ophthalmology & Visual Science

Briefly, reads were demultiplexed using 10-base well and plate barcodes, then aligned to the human transcriptome (GRCh38 reference index, Ensembl annotations) with STAR. Unique alignments were further demultiplexed by transcript UMIs, which were counted as raw gene counts. CPM matrices were derived from raw counts and used for hierarchical clustering, heatmap visualization, and principal component analysis (PCA). For normalization, variance-stabilizing transformation (VST) was applied: log(variance) was fitted against log(mean) with loess, expected variance was calculated from the observed mean, and normalized expression values were used to compute variance.

Western Blotting

Cells were lysed in RIPA buffer (Epizyme, PC101, China) containing protease and phosphatase inhibitors (Epizyme, China), incubated on ice for 30 minutes, and centrifuged at 10,000×*g* for 15 minutes at 4°C. Protein concentration was determined with the Omni-Rapid Protein Quantification Kit (Epizyme, ZJ103, China) using a microplate reader. Equal protein amounts were mixed with Omni-Easy Instant Loading Buffer (Epizyme, LT101S, China), denatured at 100°C for 10 minutes, separated by SDS-PAGE (85 V, 60–90 minutes), and transferred to PVDF membranes (Millipore, ISEQ00010) at 300 milliampere (mA) constant current. Membranes were blocked with 5% skim milk (Beyotime, P0216, China) in Tris-buffered saline-Tween 20 (TBST) for 2 hours at room temperature, incubated with primary antibodies in antibody dilution buffer (Epizyme, PS119, China) overnight at 4°C, washed, and probed with secondary antibodies for 1 hour at room temperature. Signals were detected using ECL kit (Beyotime, P10018S, China) and imaged; band intensities were quantified with ImageJ software.

Cell Viability Analysis

After the cells' attachment, 10 µL of CCK8 reagent (Yeasen, 40203ES60, China) was added to each 100 µL of medium. Following a 1 hour of incubation at 37°C under 5% CO_2, absorbance was measured at 450 nm using an enzyme meter and calculated as: (sample – blank) / (negative control – blank) × 100.

Surgical Procedures

Mice were anesthetized, and the periocular area was disinfected three times with iodine swabs. Carbomer gel was applied to the contralateral eye for protection. Under a surgical microscope, a temporal conjunctiva incision was made, and the optic nerve was exposed by blunt dissection through orbital fat and vascular sinus. The nerve was crushed at 5 mm posterior to the globe using reverse micro forceps for 10 seconds. Ofloxacin ointment was applied postoperatively to prevent infection. Mice were placed on a heating pad until recovery with body temperature and ocular surface moisture maintained throughout.

Retina Flat-Mount Preparation and Survival Count of RGCs

Mice were anesthetized with intramuscular Zoletil 50. Eyes were enucleated, rinsed briefly with PBS, and fixed in 4% PFA for 2 hours at room temperature. After PBS washes (3 × 5 minutes), the cornea and lens were removed, and the retina was dissected into a four-leaf clover shape. Retinas were flat-mounted on glass slide, fixed in cold methanol for 5 minutes, and followed by an additional 10 minutes methanol fixation in 24-well plates. Samples were washed in PBS and blocked overnight at 4°C in blocking buffer. After immunofluorescence with the RBPMS, 4-leaf clover shaped retinas were imaged with a 20 × objective using a Zeiss confocal microscope. A total of 12 locations were selected, including 4 each in the central area, pericentral area, and peripheral area. Finally, the number of RGCs in three areas was calculated as the average for four locations by ImageJ software.

Statistical Analysis

GraphPad Prism 9 (GraphPad) was used for statistical analyses. Data are presented as the mean ± standard deviation (SD). Group differences were analyzed using 1-way ANOVA followed by Tukey's post hoc test, with significance set at $P < 0.05$.

Results

Reactive Astrocytes Induced by TNF, IL-1α, and C1q Exhibit Cytotoxicity to RGCs In Vitro

Primary astrocytes were isolated and cultured from neonatal mouse brains. To avoid serum-induced alterations, which can irreversibly modify astrocytic transcriptomes[26] and minimize neuronal contamination — a serum-free culture system was utilized to obtain purified primary astrocytes.[27] Cellular identity and purity were initially assessed by RT-qPCR (Supplementary Fig. S1) and immunofluorescence staining (Fig. 1A), confirming an astrocyte purity of approximately 90% (Fig. 1B). To determine their suitability for modeling reactive astrocytes, the cells were exposed to inflammatory stimuli. As reported by Liddelow et al., the combined action of TIC, secreted by activated microglia, is both necessary and sufficient to induce A1 astrocytes13. Upon TIC exposure, physiological astrocytes developed a pronounced reactive phenotype, as evidenced by increased mRNA expression of A1-specific markers, including complement component 3 (C3d), guanylate-binding protein 2 (Gbp2), histocompatibility 2D region locus 1 (H2-d1), and histocompatibility 2T region locus 23 (H2–t23; Fig. 1C). These transcriptional changes were corroborated at the protein level (Figs. 1D–F), and immunofluorescence analysis further demonstrated robust GBP2 expression in TIC-induced astrocytes (Figs. 1G, 1H). Functionally, the cytotoxic of TIC-induced reactive astrocytes toward RGCs was confirmed using a co-culture system with whole retina dissociates. Compared with physiological astrocytes, TIC-induced reactive astrocytes markedly reduced RGC axonal length (Figs. 1I, 1J). These findings align with previous reports, supporting that TIC stimulation drives a reactive astrocyte phenotype characterized by elevated expression of A1-specific markers.

Establishment of a Screening Platform for Small Molecules Targeting Pathological Reactive Astrocytes

Given the pivotal role of reactive astrocytes in amplifying inflammation in traumatic optic neuropathies, they

Investigative Ophthalmology & Visual Science

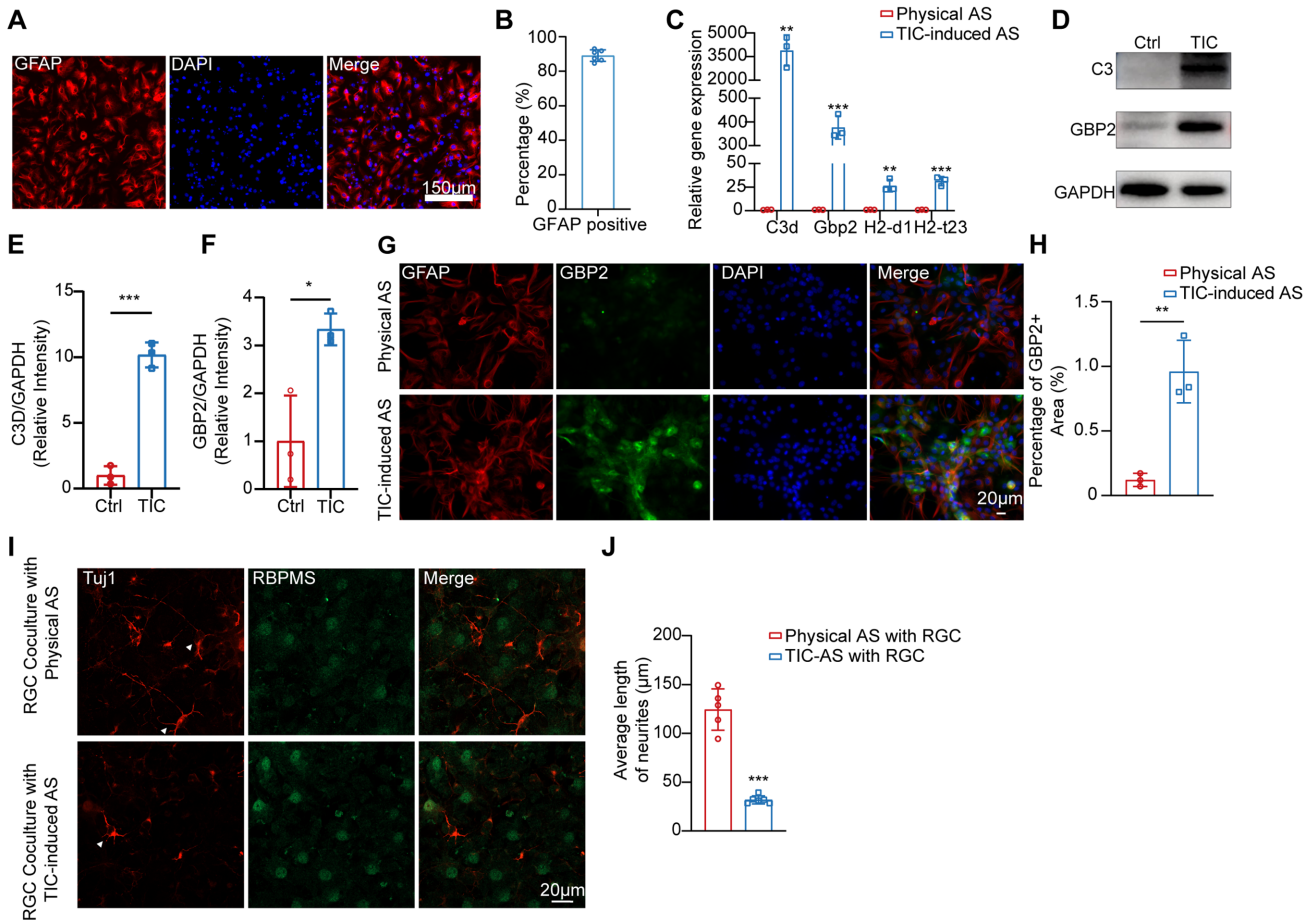

Figure 1. Identification of physiological primary astrocytes and A1 astrocytes. (**A**) GFAP immunofluorescence staining for identification of primary physiological astrocytes, *scale bar* = 150 μm. (**B**) GFAP/DAPI verifies primary physiological astrocyte purity of approximately 90% (n = 3/group). (**C**) TIC-induced astrocytes compared with physical astrocytes, the expression of A1 astrocyte markers C3d, Gbp2, H2–d1, and H2–t23 were markedly elevated (n = 3/group). (**D**) The expression trend of protein C3 and Gbp2 was consistent with that of gene expression. (**E, F**) Quantitative plot of Western blotting (n = 3/group). (**G**) The trend of GBP2 immunofluorescence assay was consistent with that of immunoblotting, *scale bar* = 20 μm. (**H**) Quantitative plot of immunofluorescence intensity (n = 3/group). (**I**) Compared with physiological astrocytes, the axons (Tuj1) of RGCs were significantly shortened after 24 hours of co-culture with TIC-induced astrocytes, *scale bar* = 20 μm. (**J**) Quantitative statistical plot of RGC mean axon length (n = 5/group).

represent a promising therapeutic target. Therefore, identifying small molecules capable of modulating reactive astrocytes holds substantial therapeutic potential. In this study, we established a screening platform to identify such compounds. Considering the large number of candidates in small-molecule libraries, the SiPer platform was first used to streamline compound selection, thereby improving screening efficiency and reducing workload and risk. The scRNA-seq data from both reactive and physiological astrocytes were analyzed to identify TFs associated with the reactive phenotype (Fig. 2A). Based on these factors, small-molecule candidates were predicted (Supplementary Table S2). Then, combined with additional compounds previously identified by our laboratory (Supplementary Table S3), yielding a final pool of small-molecule candidates. Each compound was pre-incubated with physiological astrocytes for 1 hour, followed by 24-hour treatment with TIC. Cell lysates were then collected and analyzed using the DRUG-seq2 platform for transcriptomic profiling (Supplementary Table S4). PCA demonstrated clear separation between the positive control and test groups (Fig. 2B), with replicates clustering tightly, indicating high-quality and consistent data suitable for further analysis. Among the candidates, Forsythoside B (FSTB; C12/D12) and the proteasome inhibitor Delanzomib (H1) clustered closely with the positive control (C1), suggesting their potential to modulate astrocyte phenotypes (Fig. 3B). RT-qPCR validation revealed that Delanzomib significantly downregulated A1-specific genes' expression (Supplementary Figs. S2A–D), whereas FSTB had no such effect (Supplementary Figs. S2E–H). These results highlight proteasome inhibitor as a promising approach for suppressing pathological reactive astrocytes.

Proteasome Inhibition Modulates Pathological Reactive Astrocytes

Given the observed effect of Delanzomib, we further investigate proteasome inhibitors as potential modulators of reactive astrocytes. Delanzomib is an orally bioavailable inhibitor of the chymotrypsin-like activity of the proteasome and is known to induce apoptosis in cancer cells through NF-κB pathway inhibition. Despite its potent anti-angiogenic and anticancer properties, its inability to cross the BBB limits its applicability in CNS models. Therefore, Marizomib, a BBB-permeable proteasome inhibitor, was selected for

Investigative Ophthalmology & Visual Science

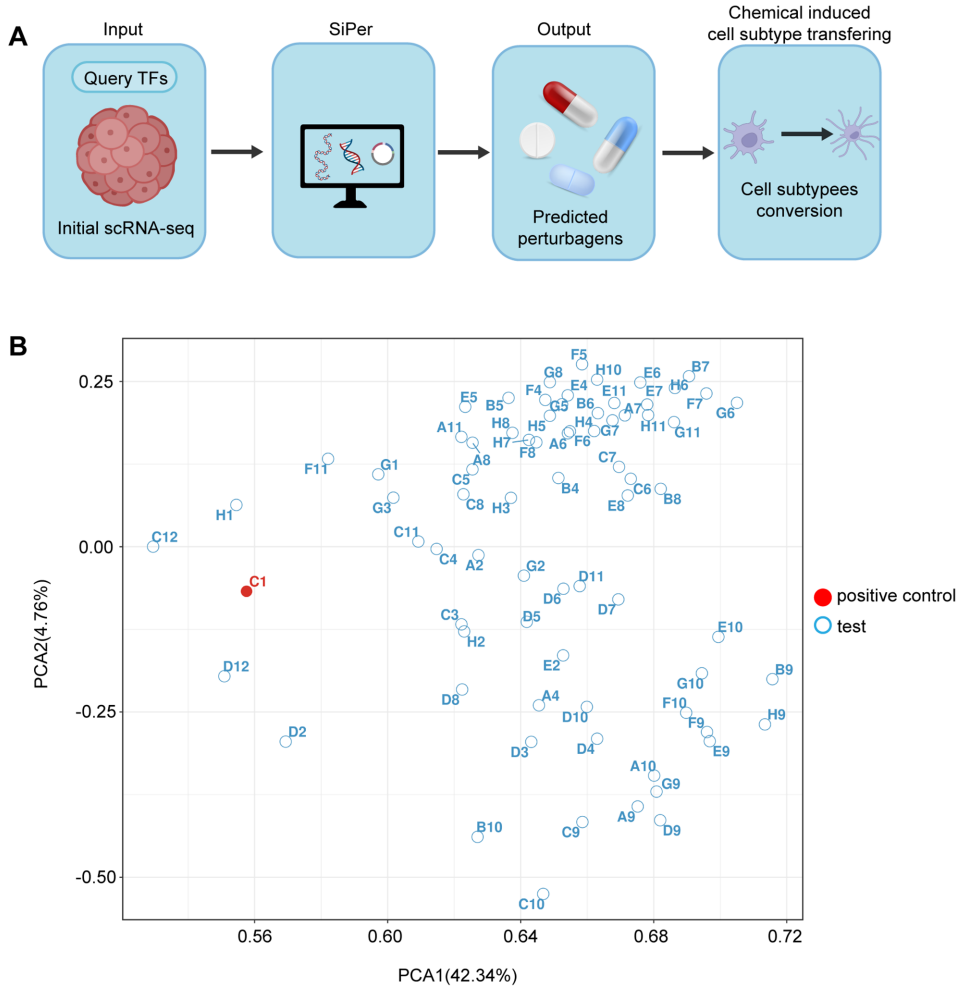

Figure 2. Establishment of a drug screening platform. (**A**) Schematic diagram of the process of the SiPer drug screening platform. (**B**) PCA plot of DRUG-seq2 for initial sequencing evaluation of the screening drug. *Red solid circles* represent the positive control, indicating resting astrocytes. *Blue hollow circles* represent A1-type astrocytes induced by TIC pretreated with different small molecules.

subsequent in vivo experiments targeting the optic nerve. RNAseq analysis revealed that Marizomib treatment significantly downregulated the expression of pathological reactive astrocyte markers while upregulating genes associated with A2-type neuroprotective astrocytes (Figs. 3A–C). RT-qPCR results corroborated these findings, showing consistent changes in both A1 and A2 gene expression (Figs. 3G, 3H). Immunofluorescence shows that the protein level of GBP2 significantly reduced by treatment of Marizomib (see Figs. 3D, 3E). Western blot analysis further demonstrated reduced protein levels of A1 markers C3 and GBP2 following Marizomib treatment (Figs. 3F, 3I). Collectively, these results indicate that proteasome inhibition not only suppresses pathological phenotypes of reactive astrocytes but also promotes the expression of gene associated with neuroprotective astrocytes.

Effects of Proteasome Inhibition on Astrocyte Reactivity and RGC Survival Following Optic Nerve Crush

To evaluate the in vivo effects of proteasome inhibitors, a mouse optic nerve crush (ONC) model was used. Immunofluorescence staining revealed increased GBP2 expression in optic nerves at days 7 and 14 post-injury, whereas no increase was observed in sham-operated mice (Fig. 4A). Quantitative analysis using ImageJ software confirmed significantly higher GBP2 fluorescence intensity in the injured groups compared with controls (Fig. 4B), indicating astrocyte activation following ONC. Regarding RGC survival, RGC numbers remained largely unchanged at days 1 and 3 post-injury. However, by days 7 and 14, there was a marked reduction in RGC density (Fig. 4C). Quantitative analysis showed that in the sham group, average RGC densities in the central, pericentral, and peripheral retina were approximately 3802/mm^2, whereas these values decreased to 1542/mm^2 at day 7 and further declined to 814/mm^2 at day 14 post-injury — both statistically significant compared with the sham group (Fig. 4E). No significant differences were observed at days 1 and 3 post-injury. These results indicate that substantial RGC loss occurs between days 7 and 14 following ONC.

Based on these findings, Marizomib was administered intravitreally at two doses (3 ng and 15 ng) to ONC-injured eyes. Immunofluorescence staining demonstrated that, at the low concentration of 3 ng, the number of GBP2-positive cells was significantly reduced in the Marizomib-treated

Investigative Ophthalmology & Visual Science

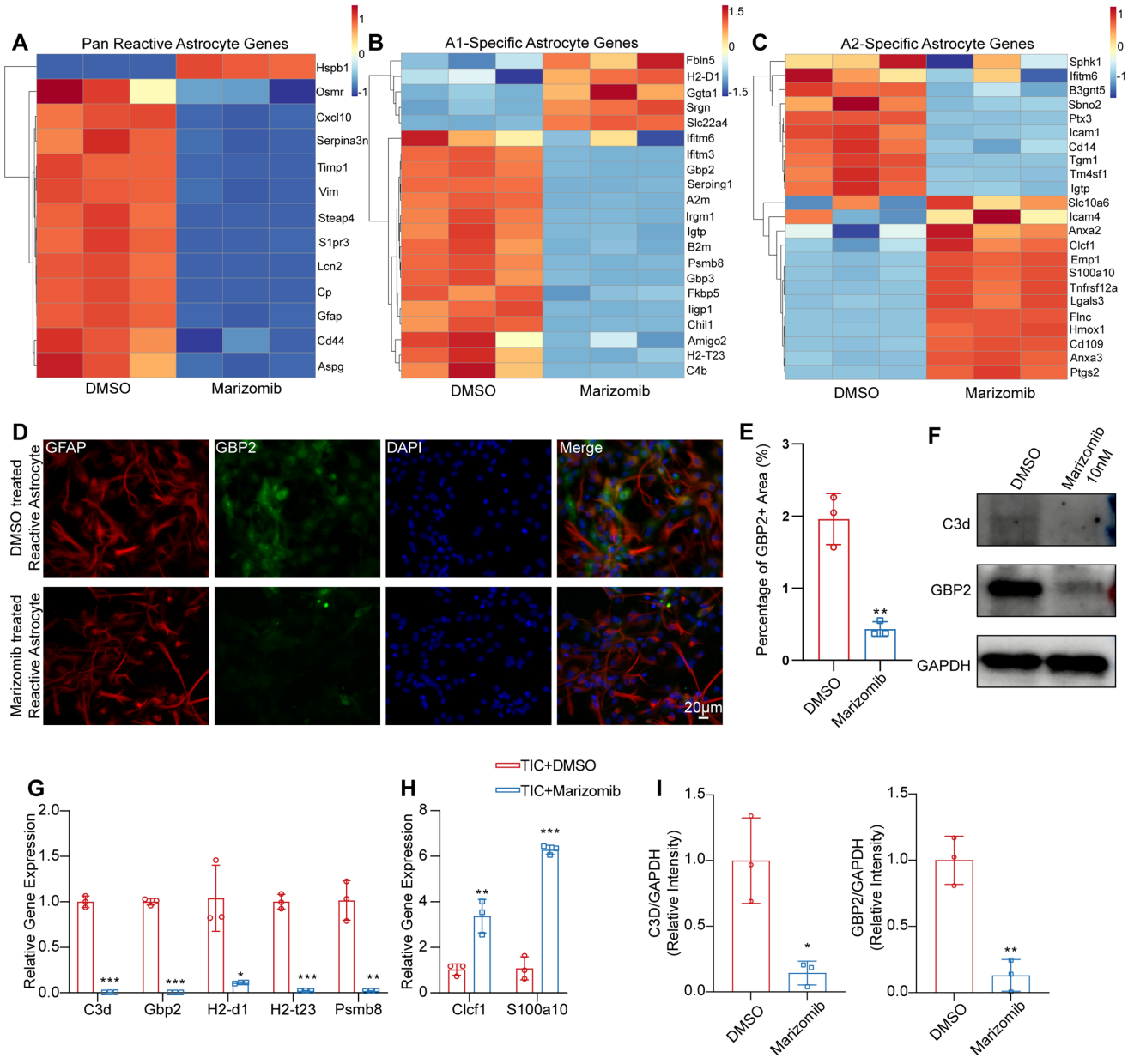

Figure 3. Marizomib alters the cellular phenotype of reactive astrocytes. Heatmaps of RNA-seq results comparing the Marizomib-treated group and the DMSO control group. (**A**) Genes associated with pan-reactive astrocytes were generally downregulated in the Marizomib-treated group. (**B**) Most A1-type astrocyte-specific genes were downregulated following Marizomib treatment. (**C**) A subset of A2-type astrocyte-specific genes was upregulated in the Marizomib-treated group. (**D**) Immunofluorescence staining of GBP2. The GBP2 protein expression was decreased in the Marizomib-treated group, *scale bar* = 20 μm. (**E**) Quantification of GBP2 fluorescence intensity (n = 3/group). (**F**) Western blot analysis. Expression levels of A1-type astrocyte-associated proteins C3d and GBP2 were downregulated in the Marizomib-treated group. The qPCR statistical analysis comparing the Marizomib-treated group and the DMSO control group. (**G**) The expression of A1-type astrocyte-related genes was significantly reduced after Marizomib treatment (n = 3/group). (**H**) the expression of A2-type astrocyte-related genes was increased in the Marizomib-treated group (n = 3/group). (**I**) Quantitative analysis of the Western blot results (n = 3/group).

groups at days 7 and day 14 post-injury compared with the vehicle-treated group (10% DMSO; Figs. 5A, 5B). Quantitative analysis confirmed a significant reduction in GBP2 fluorescence intensity in the treated groups at both time points (Figs. 5C, 5D). Given that RGC loss became apparent at day 7 in earlier experiments, we focused on days 7 and 14 for RGC quantification. RBPMS immunostaining of retinal flat mounts showed that at day 14, the 3 ng Marizomib group had a significant higher number of RBPMS-positive cells than the DMSO control group, however, no significant difference was observed at day 7, and the 15-ng dose did not confer a significant increase at either time point (Figs. 5E–G).

These results suggest that Marizomib modulates reactive astrocytes phenotypes in the injured optic nerve. Additionally, they reveal a modest, dose-dependent, and time-limited effect of Marizomib on RGC survival, warranting further investigation.

Investigative Ophthalmology & Visual Science

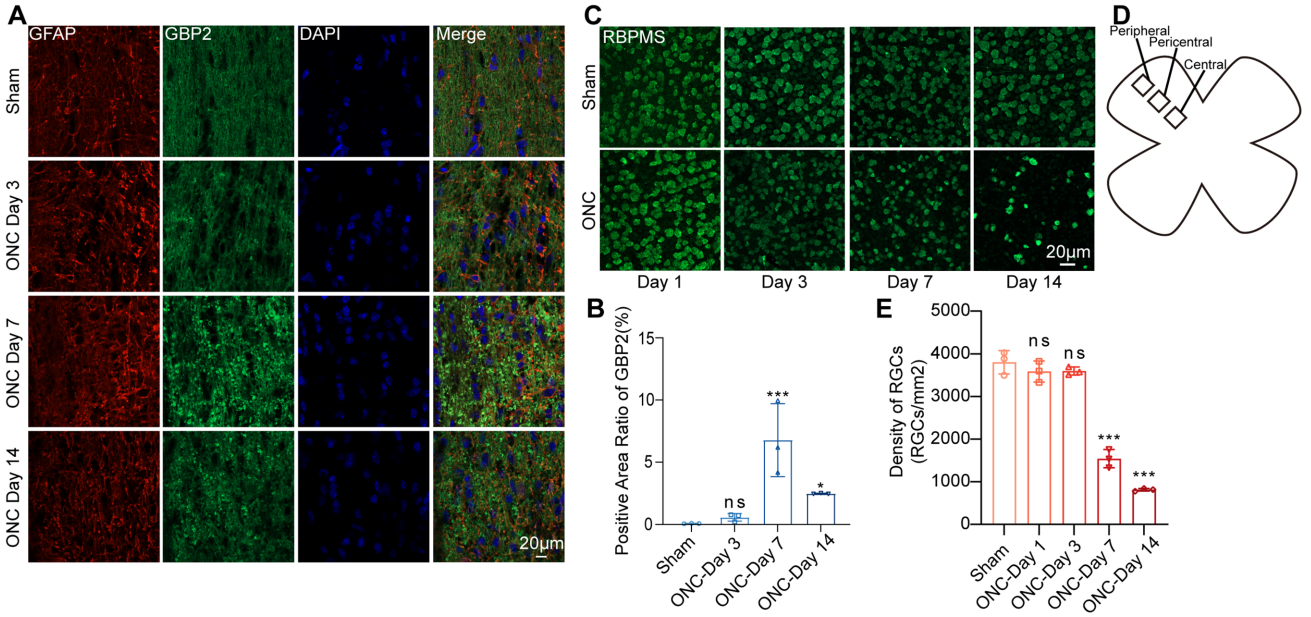

Figure 4. Changes in RGC number and optic nerve astrocyte phenotypes in the ONC mouse model. (**A**) Representative immunofluorescence images of optic nerve cryosections, *scale bar* = 20 μm. (**B**) Quantification of GBP2-positive immunofluorescence area in optic nerve sections (n = 3/group). (**C**) Representative images of pericentral of retinal flat mounts with RBPMS immunofluorescence staining, *scale bar* = 20 μm. (**D**) A diagram of retina flat mount, three boxes represent peripheral, pericentral, and central in one leaf of the whole retina, respectively. (**E**) Quantification of RBPMS-positive cell numbers (n = 3/group).

Discussion

Reactive astrocytes exhibit high levels of heterogeneity and plasticity in response to CNS injury and disease. Astrocyte activation after optic nerve injury plays a dual role: the A1 phenotype exacerbates neuroinflammation, whereas the A2 phenotype contributes to neuroprotection.[13] Although growing consensus in the field suggests that reactive astrocytes do not conform to a simple binary classification, and display a continuum of molecular and functional states that are dynamically shaped by pathological context, spatiotemporal factors, and intercellular communication.[14] Despite this paradigm shift, markers such as C3 and S100A10 remain useful indicators of specific astrocyte response associated with neuroinflammation and repair, respectively. In this study, we utilize these markers not as definitive proof of discrete phenotypes, but as molecular readouts to assess the impact of Marizomib on the astrocyte reactive state. Our qPCR and Western blot analysis revealed that Marizomib markedly downregulated A1-specific markers, such as C3 and GBP2, while upregulating A2-associated markers including S100A10 and CD109. These results suggest that Marizomib may serve as a promising therapeutic candidate for regulating astrocyte phenotypic transition. Immunofluorescence staining further demonstrated a pronounced reduction in GBP2 expression in optic nerve tissues from treated mice, indicating that Marizomib attenuates astrocyte overactivation and excessive inflammatory responses. Given the essential role of RGCs as conduits for visual signal transmission, their survival is critical for functional recovery following optic nerve injury. Our data showed significant higher number of RBPMS-positive RGCs in the Marizomib-treated group compared with controls, suggesting a potential association with RGC survival that warrants further investigation.

Currently, efficient screening methods for small molecules that induce astrocyte phenotypic transition remain limited. Most studies have relied on repurposing existing clinical drugs with known neuroprotective potential. For instance, in 2023, Telmisartan, an antihypertensive agent, was reported to modulate astrocyte phenotypes following reactive activation.[28] Other studies have shown that Rho gene knockdown can facilitate the transition from A1 to A2 phenotypes,[17] and that Fasudil, a known Rho inhibitor with neuroprotective properties, may also influence astrocyte polarization.[29] More recently, a large-scale screening of 3000 small molecules identified an HDAC3 inhibitor capable of modulating reactive astrocytes.[27] However, such approaches require substantial resources and may be limited when the compound library lacks sufficient diversity. In contrast, our AI-guided and DRUG-seq2 based platform significantly reduced screening costs, making it a practical strategy for small-scale drug discovery.

Protein degradation is a fundamental cellular function, and its dysregulation is implicated in numerous diseases. The two major intracellular protein degradation systems are the ubiquitin-proteasome system (UPS) and autophagy, which are closely interconnected. The UPS has drawn considerable attention in the context of neurodegenerative diseases, such as Alzheimer's and Parkinson's disease.[30] It is noteworthy that the effects of proteasome inhibitors on astrocyte reactivity are not uniform and appear to be context-dependent. For example, it is demonstrated that the proteasome inhibitor bortezomib reduced LCN2 production and suppressed a pro-inflammatory transcriptional profile in LPS-stimulated astrocytes, ultimately alleviating neuronal damage.[31] Similarly, Jin-Sil Bae et al. reported that systemic bortezomib administration reduced brain Lcn2 levels and dampened the expression of pro-inflammatory markers in an LPS-induced neuroinflamma-

Investigative Ophthalmology & Visual Science

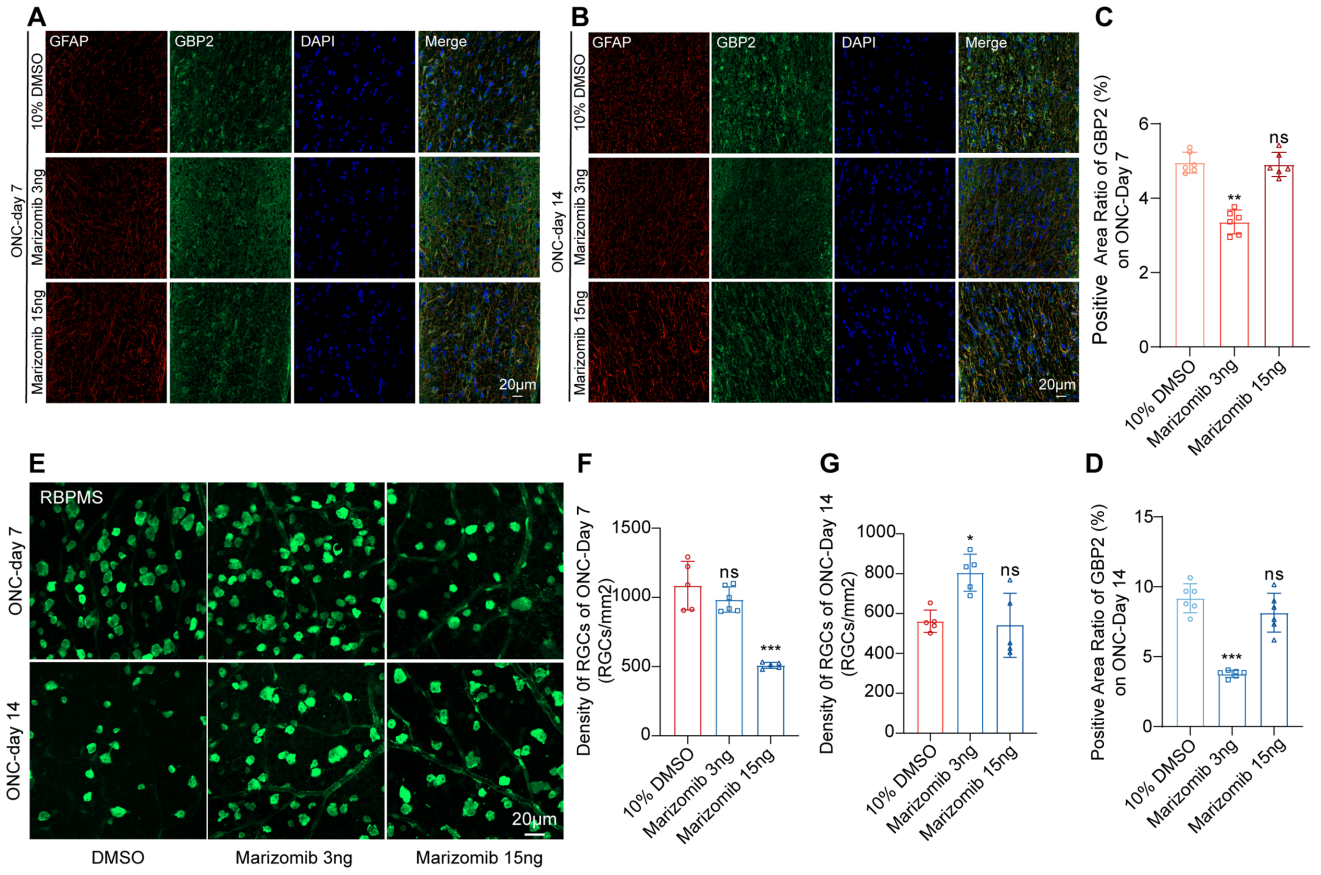

Figure 5. Effects of Marizomib on astrocyte phenotype conversion in the optic nerve and protection of RGCs. (**A**) Representative immunofluorescence images of optic nerve cryosections showing GFAP and GBP2 expression 7 days after intravitreal injection of Marizomib following ONC, *scale bar* = 20 μm. (**B**) Representative immunofluorescence images of optic nerve cryosections showing GFAP and GBP2 expression 14 days after intravitreal injection of Marizomib following ONC, *scale bar* = 20 μm. (**C**) Quantification of relative GBP2-positive fluorescence area corresponding to panel **A** (n = 5/group). (**D**) Quantification of relative GBP2-positive fluorescence area corresponding to panel **C** (n = 6/group). (**E**) Representative images of pericentral of retinal flat mounts with RBPMS immunofluorescence staining, *scale bar* = 20 μm. (**F**) Quantification of RBPMS-positive cells in retinal flat mounts 7 days after intravitreal injection of different concentrations of Marizomib following ONC (n = 5/group). (G) Quantification of RBPMS-positive cells in retinal flat mounts 14 days after intravitreal injection of different concentrations of Marizomib following ONC (n = 6/group).

tion mouse mode.[32] These studies suggest that, under specific inflammatory conditions, proteasome inhibition can suppress pro-inflammatory responses in astrocytes. Our results showed that the proteasome inhibitor Marizomib altered the transcriptional profile of reactive astrocytes, suppressing A1 marker genes induced by TIC stimulation while enhancing A2 marker gene expression. This suggests that proteasome inhibition may shift TIC-induced astrocytes toward an A2-like transcriptional phenotype. We therefore propose a potential mechanism in which proteasome inhibitors downregulate neurotoxic A1-associated genes and upregulate A2 gene expression. However, the effects of different proteasome inhibitors may vary across disease models, depending on the upstream stimuli, cellular state, and interaction networks. Nonetheless, it is important to note that proteasome inhibition can also cause the accumulation of misfolded proteins and, in severe cases, induce apoptosis,[30] which may explain why we did not achieve the goal of preserving RGCs with higher concentration. Thus, the protective effect of Marizomib in optic nerve injury may represent a beneficial mode of astrocyte modulation by proteasome inhibitors within a specific microenvironment.

Optic nerve injury is characterized by the intrinsic inability of RGCs to regenerate, and its repair remains highly complex.[33] Current treatment strategies – including the administration of neurotrophic factors, stem cell transplantation, and gene therapy – face significant challenges, such as immune rejection and low bioavailability. The development of safe and effective pharmacological interventions is therefore a key goal in optic nerve injury research. Our study shows that the proteasome inhibitor Marizomib facilitates the transition of astrocytes toward a neuroprotective phenotype, these findings suggest that proteasome inhibition can modulate astrocyte reactivity at the molecular level, providing a basis for further investigation into its potential therapeutic applications.

Despite these promising results, several limitations remain. The precise molecular targets of proteasome inhibition in astrocyte modulation require further elucidation. Future studies should integrate multi-omics analyses and functional validation to systematically dissect the specific signaling pathways and key nodes through which Marizomib modulates astrocyte states in the optic nerve injury microenvironment. It is also important to note that the effect of Marizomib on RGC survival was modest and observed only at a

Investigative Ophthalmology & Visual Science

single dose and time point. Therefore, whereas Marizomib effectively modulates astrocyte reactivity, whether this translates into meaningful RGC protection requires further validation with larger sample sizes and additional time points. Moreover, our findings are currently limited to small animal models; validation in large animal models or human optic nerve injury is necessary to confirm both efficacy and safety. In addition, optimizing the delivery method is critical to minimize secondary injury while maximizing bioavailability and therapeutic benefit. Future studies should investigate the application of proteasome inhibitors in other neurological injury models, such as spinal cord injury and neurodegenerative diseases including Alzheimer's. Combining Marizomib with advanced drug delivery systems – such as nanocarriers or hydrogel systems – may further enhance its targeting precision and therapeutic efficacy.

Acknowledgments

Supported by the National Key Research and Development Program of China (2021YFA1101202) and the National Natural Science Foundation of China (82471052).

Disclosure: **T. Li**, None; **H. Peng**, None; **N. Wu**, None; **M. Zhu**, None; **Z. Li**, None; **Q. Dai**, None; **M. Jin**, None; **S. Pan**, None; **W. Wu**, None

References

1. Yan W, Chen Y, Qian Z, et al. Incidence of optic canal fracture in the traumatic optic neuropathy and its effect on the visual outcome. *Br J Ophthalmol*. 2016;101:261–267.
2. Guy WM, Soparkar CNS, Alford EL, Patrinely JR, Sami MS, Parke RB. Traumatic optic neuropathy and second optic nerve injuries. *JAMA Ophthalmol*. 2014;132:567.
3. Yu B, Ma Y, Tu Y, Wu W. The outcome of endoscopic transethmosphenoid optic canal decompression for indirect traumatic optic neuropathy with no-light-perception. *J Ophthalmol*. 2016;2016:6492858.
4. Wladis EJ, Aakalu VK, Sobel RK, et al. Interventions for indirect traumatic optic neuropathy. *Ophthalmology*. 2021;128:928–937.
5. Goulart CO, Mendonça HR, Teixeira Oliveira J, et al. Repulsive environment attenuation during adult mouse optic nerve regeneration. *Neural Plast*. 2018;2018:5851914.
6. Zhang S, Liu B, Zhu H, et al. A novel rat model with long range optic nerve injury to study retinal ganglion cells endogenous regeneration. *Neuroscience*. 2021;465:71–84.
7. Verkhratsky A, Parpura V, Vardjan N, Zorec R. Physiology of astroglia. *Neurodegener Dis*. 2020;1175:45–91.
8. Endo F, Kasai A, Soto JS, et al. Molecular basis of astrocyte diversity and morphology across the CNS in health and disease. *Science*. 2022;378:eadc9020.
9. Brandebura AN, Paumier A, Onur TS, Allen NJ. Astrocyte contribution to dysfunction, risk and progression in neurodegenerative disorders. *Nat Rev Neurosci*. 2023;24:23–39.
10. Clarke LE, Liddelow SA. Diversity reaches the stars. *Nature*. 2017;548:396–397.
11. Bazargani N, Attwell D. Astrocyte calcium signaling: the third wave. *Nat Neurosci*. 2016;19:182–189.
12. Zamanian JL, Xu L, Foo LC, et al. Genomic analysis of reactive astrogliosis. *J Neurosci*. 2012;32:6391–6410.
13. Liddelow SA, Guttenplan KA, Clarke LE, et al. Neurotoxic reactive astrocytes are induced by activated microglia. *Nature*. 2017;541:481–487.
14. Escartin C, Galea E, Lakatos A, et al. Reactive astrocyte nomenclature, definitions, and future directions. *Nat Neurosci*. 2021;24:312–325.
15. Fei X, Dou YN, Wang L, et al. Homer1 promotes the conversion of A1 astrocytes to A2 astrocytes and improves the recovery of transgenic mice after intracerebral hemorrhage. *J Neuroinflammation*. 2022;19:67.
16. Xu X, Zhang A, Zhu Y, et al. MFG-E8 reverses microglial-induced neurotoxic astrocyte (A1) via NF-κB and PI3K-Akt pathways. *J Cell Physiol*. 2019;234:904–914.
17. Liu C, Shen L, Xu L, Zhu A, Huang Y. Ror2 mediates chronic post-thoracotomy pain by inducing the transformation of A1/A2 reactive astrocytes in rats. *Cell Signal*. 2022;89:110183.
18. Cheng L, Gao L, Guan W, et al. Direct conversion of astrocytes into neuronal cells by drug cocktail. *Cell Res*. 2015;25:1269–1272.
19. Hou P, Li Y, Zhang X, et al. Pluripotent stem cells induced from mouse somatic cells by small-molecule compounds. *Science*. 2013;341:651–654.
20. Ye J, Ge J, Zhang X, et al. Pluripotent stem cells induced from mouse neural stem cells and small intestinal epithelial cells by small molecule compounds. *Cell Res*. 2016;26:34–45.
21. Cao N, Huang Y, Zheng J, et al. Conversion of human fibroblasts into functional cardiomyocytes by small molecules. *Science*. 2016;352:1216–1220.
22. Cieślar-Pobuda A, Knoflach V, Ringh MV, et al. Transdifferentiation and reprogramming: overview of the processes, their similarities and differences. *Biochim Biophys Acta Mol Cell Res*. 2017;1864:1359–1369.
23. Zheng M, Xie B, Okawa S, Liew SY, Deng H, del Sol A. A single cell-based computational platform to identify chemical compounds targeting desired sets of transcription factors for cellular conversion. *Stem Cell Reports*. 2023;18:131–144.
24. Li J, Ho DJ, Henault M, et al. DRUG-seq provides unbiased biological activity readouts for neuroscience drug discovery. *ACS Chem Biol*. 2022;17:1401–1414.
25. Cameron EG, Nahmou M, Toth AB, et al. A molecular switch for neuroprotective astrocyte reactivity. *Nature*. 2025;626:574–582.
26. Foo LC, Allen NJ, Bushong EA, et al. Development of a method for the purification and culture of rodent astrocytes. *Neuron*. 2011;71:799–811.
27. Clayton BLL, Kristell JD, Allan KC, et al. A phenotypic screening platform for identifying chemical modulators of astrocyte reactivity. *Nat Neurosci*. 2024;27:656–665.
28. Quan W, Xu CS, Li XC, et al. Telmisartan inhibits microglia-induced neurotoxic A1 astrocyte conversion via PPARγ-mediated NF-κB/p65 degradation. *Int Immunopharmacol*. 2023;123:110761.
29. Guo M-F, Meng J, Li YH, et al. The inhibition of Rho kinase blocks cell migration and accumulation possibly by challenging inflammatory cytokines and chemokines on astrocytes. *J Neurol Sci*. 2014;343:69–75.
30. Obeng EA, Carlson LM, Gutman DM, *H*,Lee KP, Boise LH. Proteasome inhibitors induce a terminal unfolded protein response in multiple myeloma cells. *Blood*. 2006;107:4907–4916.
31. Jung BK, Park Y, Yoon B, et al. Reduced secretion of LCN2 (lipocalin 2) from reactive astrocytes through autophagic and proteasomal regulation alleviates inflammatory stress and neuronal damage. *Autophagy*. 2023;19:2296–2317.
32. Bae JS, Heo JE, Ryu KY. Proteasome inhibition suppresses the induction of lipocalin-2 upon systemic lipopolysaccharide challenge in mice. *Mol Brain*. 2024;17:73.
33. Cen L-P, Ng TK, Liang JJ, et al. Human periodontal ligament-derived stem cells promote retinal ganglion cell survival and axon regeneration after optic nerve injury. *Stem Cells*. 2018;36:844–855.